Applied Catalysis B: Environmental 164 (2015) 82–91

Contents lists available at ScienceDirect

Applied Catalysis B: Environmental

journal homepage: www.elsevier.com/locate/apcatb

Photocatalytic degradation and electricity generation in a rotating disk photoelectrochemical cell over hierarchical structured BiOBr film

Kan Li[a], Hongbo Zhang[a], Yanping Tang[b], Diwen Ying[c], Yunlan Xu[d], Yalin Wang[a], Jinping Jia[a,*]

[a] School of Environmental Science and Engineering, Shanghai Jiao Tong University, Shanghai 200240, PR China
[b] School of Chemistry and Chemical Engineering, Shanghai Jiao Tong University, Shanghai 200240, PR China
[c] School of Materials Science and Engineering, Shanghai Jiao Tong University, Shanghai 200240, PR China
[d] School of Chemical Engineering, Chongqing University of Technology, Chongqing 400050, PR China

ARTICLE INFO

Article history:
Received 24 July 2014
Received in revised form 1 September 2014
Accepted 5 September 2014
Available online 16 September 2014

Keywords:
Immobilized photocatalyst
Hierarchical structure
Light utilization efficiency
Visible light photocatalysis
Electricity generation

ABSTRACT

A double hierarchical structured BiOBr film was prepared on Ti substrate through hydrolysis of Bi_2O_3 film in the presence of Br^- and H^+. The prepared BiOBr film exhibited much better photocatalytic (PC) activity on Rhodamine B (RhB) degradation than Bi_2O_3 film in a rotating disk PC reactor. The double hierarchical structure could not only enhance the surface area, but also exhibited strong RhB adsorption capacity and high light utilization efficiency due to multiple reflections of incident light. Due to similar hierarchical structure, BiOCl film was also used to compare the PC activity of BiOBr film. Because the band gap energy of BiOBr (2.5 eV) was narrower than that of BiOCl (3.2 eV), weaker PC activity was obtained for BiOBr film under UV light. However, besides RhB photosensitization degradation, BiOBr could also be excited by part of visible light to generate •OH, resulting in a better RhB removal under visible light. A Pt cathode was further connected to BiOBr/Ti photoanode to establish a rotating disk BiOBr/Ti–Pt photoelectrochemical cell to generate electricity with the degradation of pollutants simultaneously. 0.77 and 0.74 V open-circuit voltage, 0.019 and 0.010 mA cm^{-2} short-circuit current density were obtained under UV and visible light irradiation, respectively, with 50 mL 5 mg L^{-1} RhB as "fuel". The PC activity was also improved due to the efficient separation of electrons and holes. The total current generated was stable but gradually decreased with treatment time due to the consumption of "fuel".

1. Introduction

After more than 40 years development, photocatalytic (PC) technique has been widely applied in air purification [1], self-cleaning surface [2], fresh product storage [3] and anti-fogging [4]. However, in the field of water treatment, the application of PC technique is still restricted due to the low light utilization efficiency [5]. A lot of works have been done to enhance the light utilization efficiency in the past few years, from PC reactor design to new photocatalyst synthesis. In macro aspect, the thin liquid film PC reactor can effectively reduce light loss caused by solution absorption [6,7]. To further change the planar substrate to wedge or pyramid structures can not only enlarge PC surface area, but also enhance light utilization efficiency due to multiple reflection of incident light [8,9]. In micro aspect, photocatalysts with light-harvesting morphologies such as flower-like structure [10], hollow sphere [11] and core-shell structure [12] have also been synthesized, among which, bismuth oxyhalides (BiOX; X = Cl, Br) have attracted intensive attention in recent years because of their high PC activity and layered crystal structure [13–15]. This layered structure can not only separate the electron–hole pairs efficiently, but can also easily be utilized to built other special 3D structures to capture more incident light. Zhang et al. have synthesized BiOCl nestlike and hollow spheres by hydrolyzing $BiCl_3$ with the addition of PVP and citric acid and the 3D structures could effectively improve PC activity on Rhodamine B (RhB) degradation under UV irradiation [16]. Huo et al. have prepared flower-like BiOBr microspheres via slovothermal method with CTAB as surfactant and Br source [17]. The obtained samples exhibited excellent photodegradation of dye due to the enhanced visible light absorbance via the light multiple reflections, the efficient separation of photo-generated electrons and holes, the high crystallization and the large surface area. However, considering the difficulty in recovery of dispersed photocatalysts in real wastewater treatment application, to develop a simple and

* Corresponding author. Tel.: +86 21 54742817; fax: +86 21 54742817.
E-mail address: jpjia@sjtu.edu.cn (J. Jia).

http://dx.doi.org/10.1016/j.apcatb.2014.09.017
0926-3373/

environmental friendly way to prepare immobilized BiOX film with high light utilization efficiency and PC activity is still a big challenge for researchers.

In our former research, we have proposed a facile method to prepare BiOCl film on a Ti substrate via hydrolysis of Bi_2O_3 with the addition of Cl^- in acidic condition [18]. The BiOCl film owned a hierarchical structure and exhibited high PC activity on RhB degradation, which was even better than that obtained by anatase TiO_2 film. Meanwhile, because the strong adsorption was observed on the surface of BiOCl film, RhB could also be degraded under visible light irradiation through indirect photosensitization effect. However, because the band gap energy of prepared BiOCl is as large as 3.2 eV, it can not be excited by visible light, which may restrict its fully utilization of visible light or solar energy. Compares with BiOCl, BiOBr owns lower band gap energy and can be excited by part of visible light. Many researchers have reported that BiOBr exhibited much higher PC activity under visible light in comparison with BiOCl [19–21]. Besides pollutants degradation, BiOBr film was also reported to be utilized in colorimetric biosensing [22] and ultraviolet photodetection [23]. In this research, based on our former work, we have developed a facile way to prepare hierarchical structured BiOBr film on a Ti substrate and the obtained BiOBr/Ti plate was equipped on a thin film rotating disk PC reactor, which has been confirmed to be an efficient PC reactor [24], to evaluate its PC activity on RhB degradation under UV and visible light irradiation. The results were compared with those obtained by Bi_2O_3 film and BiOCl film.

In a typical PC process, the photo-generated electrons will react with O_2 to generate $O_2^{\bullet-}$ to further oxidize pollutants or to recombine with holes, which may reduce the light utilization efficiency. In order to further improve light utilization efficiency and fully utilize photo-generated electrons, a cathode such as platinum or graphite can be employed to connect with photoanode to form a photoelectrochemical cell. Photo-generated electrons will transfer to the cathode spontaneously through the external circuit due to the existing of potential difference between photoanode and cathode. In that case, besides light utilization efficiency can be enhanced via efficient separation of photogenerated electrons and holes, electricity can also be generated with PC degradation of pollutants simultaneously. Similar like a microbial fuel cell (MFC), this photoelectrochemical cell is also called photo fuel cell (PFC) [25]. Since a review article on PFC system has been published in Lianos [26], this system has gained more and more attention in recent years [27–30]. Though the electricity generated in PFC is still low in comparison with that generated by solar cells or dye-sensitized solar cells (DSSC), this electricity energy has already been utilized in photoelectrocatalysis (PEC) as bias voltage [31] or coupled with biocathode to help denitrification [32]. In this research, the electricity generation property of prepared BiOBr film was also determined in a thin film rotating disk PFC system under UV and visible light.

2. Experimental

2.1. BiOBr film preparation

All chemical reagents purchased from Shanghai Chemical Reagent Co., China, were in analytical grade without further purifications. Ti substrates (a round disk with diameter of 75 mm, thickness of 1 mm, Shanghai Hongtai Metal Production Co. Ltd., China) were burnished using abrasive paper and then ultrasonic cleaned using acetone and distilled water, respectively. The precursor solution was prepared by the following method. 4.0 g $Bi(NO_3)_3{\cdot}5H_2O$ was dissolved in 20 mL ethanol containing 1 mol L^{-1} HNO_3. After being stirred for 30 min, a transparent solution was obtained. The result solution was spin-coated onto a Ti disk. The Ti disk was then dried at 120 °C for 30 min first and further calcined at 350 °C for 2 h with heating rate of 5 °C min^{-1}. After cooling to room temperature, the light-yellow Bi_2O_3/Ti disk was obtained (Fig. S1). The BiOBr film was prepared through hydrolysis of Bi_2O_3 film in the presence of Br^- in acidic condition. Specifically, the Bi_2O_3/Ti disk was immersed in 0.05 mol L^{-1} NaBr solution with pH 2.0 (adjusted with 1 mol L^{-1} H_2SO_4) for 30 min and the BiOBr film with white color was obtained (Fig. 1(a)). In order to evaluate the PC activity of obtained BiOBr film, BiOCl/Ti disk was also prepared using NaCl instead of NaBr for comparison (Fig. S2) [18].

2.2. Characterization of BiOBr film

The BiOBr powder was sonicated down from the BiOBr/Ti disk and used for further detection of X-ray diffraction (XRD), high-resolution transmission electron microscopy (HRTEM), diffuse reflectance absorption spectra (DRS) and Zeta potential. The crystal structure of the BiOBr film was determined by XRD using a D/Max2200 diffractometer (Rigaku, Japan) at a scanning rate of 5° min^{-1} in 2θ range from 5° to 90°. The morphology of the BiOBr film was characterized by an S-2150 field emission scanning electron microscope (FESEM, Hitachi Corp., Japan) at a high voltage of 15 kV and a JSM-2010 high-resolution transmission electron microscopy (HRTEM, JEOL Ltd., Japan). The UV–vis diffuse reflectance absorption spectras (UV–vis DRS) of BiOBr and BiOCl films were recorded on a Lambda 750S UV–vis–NIR spectrophotometer (PerkinElmer, USA) in the range of 200–700 nm. The Zeta potential of the BiOBr film was determined by ZS90 Zeta Potential Analyzer (Malvern Instruments Ltd., UK). The flat-band potential of BiOBr and BiOCl films were electrochemically determined from the Mott–Schottky plots using an Autolab 4.9 system (Metrohm, Switzerland) with BiOBr/Ti or BiOCl/Ti plate as working electrode; Pt and saturated calomel electrode (SCE) as auxiliary and reference electrodes; and 0.05 mol L^{-1} NaBr or NaCl as electrolyte, respectively.

2.3. PC activity measurement

The PC activity of BiOBr film was evaluated through the degradation of Rhodamine B (RhB) using a rotating disk PC reactor under UV or visible light irradiation. The schematic diagram of the reactor was shown in Fig. S3(a). The rotating speed was set at 60 rpm which was controlled by a motor (Outai Transmission Electromechanical Co. Ltd., Shanghai, China). When the disk is rotating, only a thin solution film (μm level) is coated on the upper part of disk and incident light can irradiate on BiOBr film directly, which greatly reduces the light loss caused by solution absorption. The reactor was placed 3 cm away from the light source. An 11 W mercury lamp (Philips, 254 nm) and a 150 W xenon lamp (Shanghai Lansheng Co. Ltd., Shanghai, China) with a 400 nm cutoff filter were used as UV and visible light source, the light intensity was maintained constantly at 13 mW cm^{-2} and 50 mW cm^{-2}, respectively. 50 mL of 5 mg L^{-1} RhB (a cationic dye) solution was filled in the reactor to be treated. Before the experiment, the disk was rotated in dark for 20 min to reach adsorption–desorption equilibrium. The Bi_2O_3/Ti and BiOCl/Ti disks were also used to compare the PC activity of BiOBr film in the same condition. In order to analyze the mechanisms of PC degradation process, •OH and $O_2^{\bullet-}$ generated during the reaction were detected by adding trapping agents. 10 mmol L^{-1} *tert*-butyl alcohol (TBA) [33] and 0.1 mmol L^{-1} benzoquinone (BQ) [34] were added to capture •OH and $O_2^{\bullet-}$, respectively. Meanwhile 50 mL of 5 mg L^{-1} Methyl Orange (MO, an anionic dye) and 50 mL 5 mg L^{-1} colorless salicylic acid (SA) were also used instead of RhB to be treated under UV and visible light irradiation. The concentration of RhB, MO and SA solutions were

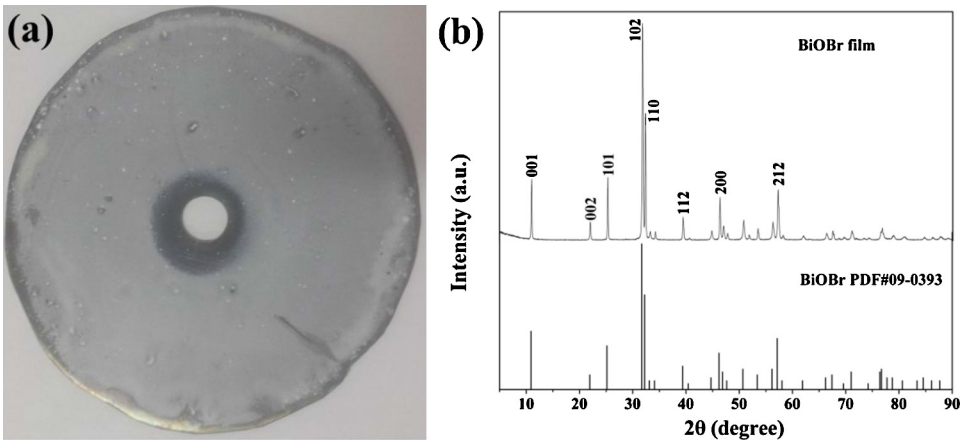

Fig. 1. (a) Photographic image of BiOBr/Ti disk and (b) XRD pattern of the BiOBr film.

determined by measuring solution absorbance at the wavelength of 563 nm, 465 nm and 297 nm, respectively, using a UV–vis spectrophotometer (UV-2102PCS, UNICO, Shanghai).

2.4. Electricity generation measurement

A Pt cathode (3 cm × 4 cm) was connected with BiOBr/Ti disk to establish a rotating disk photo fuel cell (PFC) system (Fig. S3(b)). The distance between the BiOBr/Ti disk and Pt cathode was 1 cm. 50 mL 5 mg L^{-1} RhB was used as "fuel" to be degraded under UV and visible light irradiation with 0.05 mol L^{-1} NaBr as electrolyte. Meanwhile, 50 mL 0.005 mol L^{-1} glucose, 0.05% ethanol and 0.05% acetic acid were also employed as "fuels" to evaluate the electricity generation properties in this BiOBr/Ti–Pt rotating disk PFC. The current–voltage (*J–V*) characteristics of the cell were measured by a two electrodes system using Autolab 4.9 system with BiOBr/Ti disk as working electrode; Pt cathode as auxiliary and reference electrode at the same time.

3. Results and discussion

3.1. Morphology characteristics

The phase structure of the BiOBr film was examined by X-ray diffraction (XRD). As shown in Fig. 1(b), all the diffraction peaks could be readily indexed as the tetragonal phase of BiOBr (space group: *P*4/*nmm*(129), PDF no. 09-0393) with the lattice constants of $a = b = 3.926$ Å and $c = 8.103$ Å. The diffraction peaks were sharp and no other impurity peaks were detected, indicating the high degree of crystallization and purity of the BiOBr film.

The morphology of the obtained BiOBr film was detected by the field emission scanning electron microscope (FESEM). As shown in Fig. 2(a) and (b), the flower-like hierarchical structured BiOBr

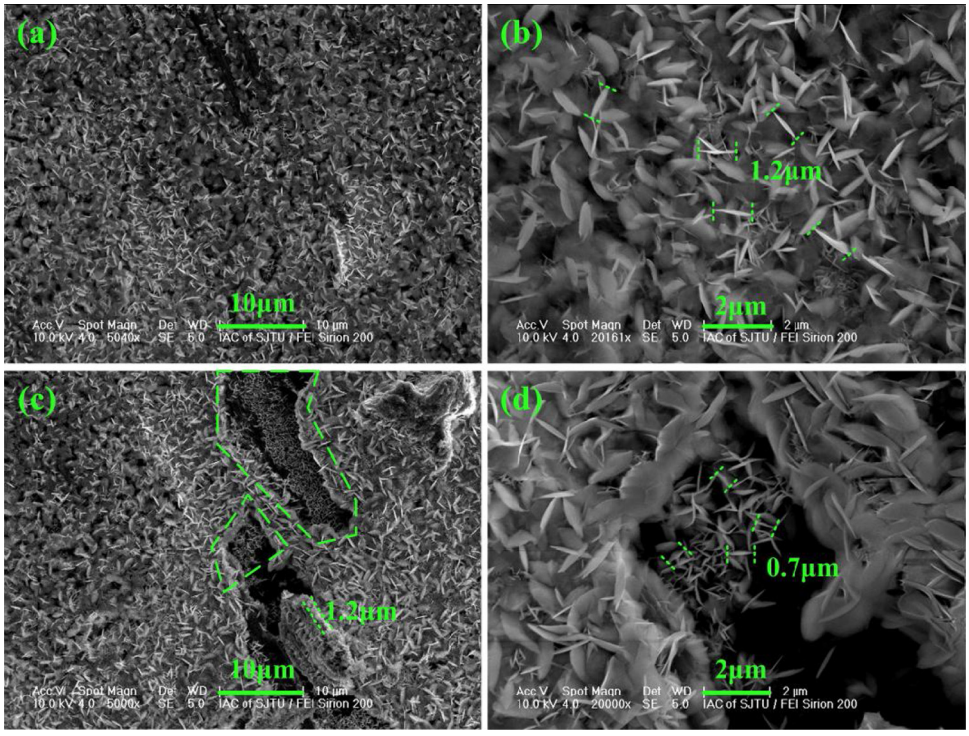

Fig. 2. FESEM images of BiOBr film. (a) Low magnification, (b) high magnification, (c) low magnification and (d) high magnification of a broken area.

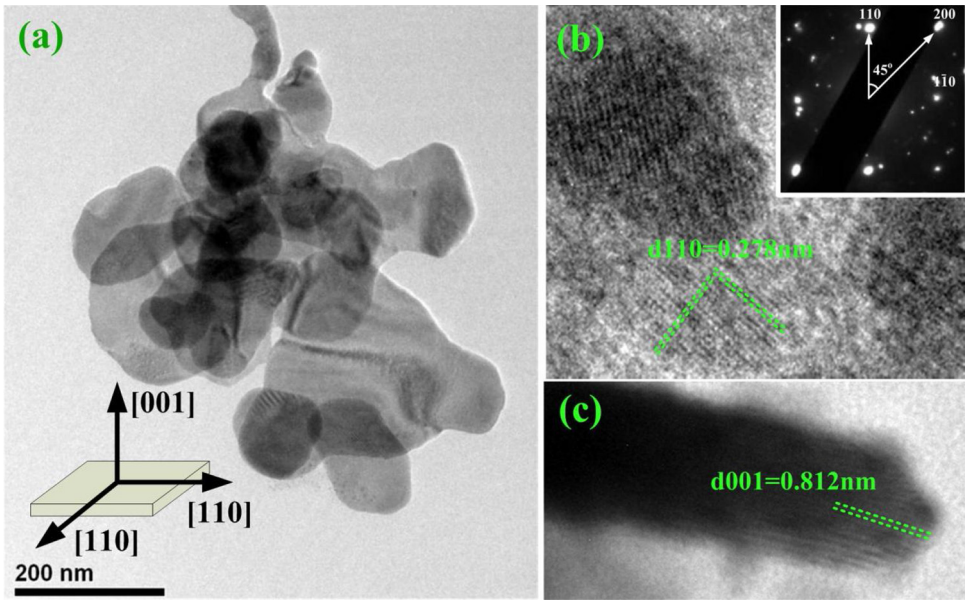

Fig. 3. (a) Low-magnification TEM image of BiOBr nanosheets (the inset is the schematic illustration of crystal orientation of BiOBr nanosheet). (b) HRTEM image and SAED pattern of the BiOBr nanosheet taken along the [0 0 1] zone axis. (c) HRTEM image of side view of a BiOBr nanosheet.

film was observed, which was composed of BiOBr nanosheets with 10 nm in thickness and 1.2 μm in plane size. Most of these nanosheets were perpendicular to the Ti substrate. Fig. 2(c) exhibited a broken area of the prepared BiOBr film. It can be observed that there were two layers of BiOBr film coated on the surface of Ti substrate and the thickness of the outer layer was 1.2 μm, which was consistent with the size of BiOBr nanosheets observed in Fig. 2(b). For the inner layer, as shown in Fig. 2(d), the size of the BiOBr nanosheets was much smaller (only 0.7 μm), making the inner layer more intensive than the outer layer. This double hierarchical structure can not only enhance surface area, but may also capture more light and improve the light utilization efficiency.

The detailed crystal structure of BiOBr nanosheets were determined by high-resolution transmission electron microscopy (HRTEM) and the results are shown in Fig. 3. After strong ultrasonication, the nanosheets were broken with different sizes and were irregular and overlapped with each other (Fig. 3(a)). The bottom and top surface of the BiOBr nanosheets were identified as {0 0 1} facets, while the four lateral surfaces were {1 1 0} facets (Fig. 3(a) inset). The HRTEM image of a single nanosheet (viewed from {0 0 1} axis) in Fig. 3(b) showed clearly two sets of lattice fringes with a lattice spacing of 0.278 nm, corresponding to that of the (1 1 0) planes. The unique pattern of diffraction spots observed in SAED pattern (Fig. 3(b) inset) could be indexed to the (1 1 0) and (2 0 0) plane, which confirmed its crystal structure. Fig. 3(c) exhibited the HRTEM image of the side wall of a nanosheet and visible lattice fringes of (0 0 1) planes with a lattice spacing of 0.812 nm were clearly observed. In BiOBr nanosheets, Bi, O and Br ions stack layer upon layer in the planes perpendicular to the {0 0 1} axis to form the five-layered unit (Br–O–Bi–O–Br), which can be considered as a planar 'macromolecule' with a weak nonbonding interlayer van der Waals interaction along the {0 0 1} axis and strong intralayer bonding along {1 1 0} axis. This special bonding structure makes the BiOBr nanosheets with large area of {001} facets exposed. It has been reported that {0 0 1} facets of BiOBr exhibited remarkably higher PC activity for oxidation of pollutants than other facets [35].

The growth mechanism of the hierarchical structured BiOBr film was preferred to be a nucleation–dissolution–recrystallization process because there were no hard or soft templates added [36]. The Bi_2O_3 on the surface would react with Br^- and H^+ to form $BiBr_3$ dissolved in water first (Eq. (1)). Then the dissolved $BiBr_3$ was hydrolyzed immediately in water to form BiOBr deposited on the surface of Bi_2O_3 and acted as nucleation centers (Eq. (2)).

$$Bi_2O_3 + 6Br^- + 6H^+ \rightarrow 2BiBr_3 + 3H_2O \quad (1)$$

$$BiBr_3 + H_2O \rightarrow BiOBr\downarrow + 2H^+ + 2Br^+ \quad (2)$$

The exposed Bi_2O_3 then was further dissolved and more BiOBr would form on the nucleation centers. The generated H^+ could easily adsorb on the O-terminated {0 0 1} facets of BiOBr, the BiOBr grew faster along the {1 1 0} orientations rather than the {0 0 1} orientations, leading to the large area of {0 0 1} facets exposed. Because the Bi_2O_3 solid nanoospheres distributed more intensive in inner part (Fig. S1(c)), new nucleation centers would form in inner part of the film, which might result in the double hierarchical structure of BiOBr film built with different sized BiOBr nanosheets.

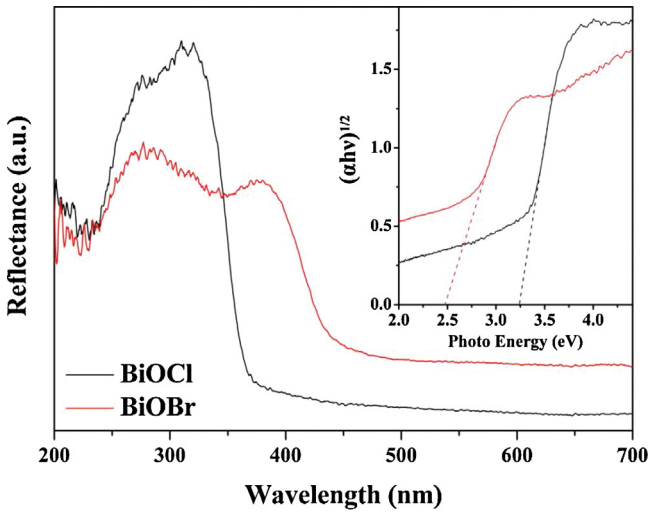

Fig. 4. The UV–vis diffuse reflectance spectrum of BiOBr and BiOCl film. The inset is the curve of $(Ah\upsilon)^{1/2}$ *vs.* $h\upsilon$.

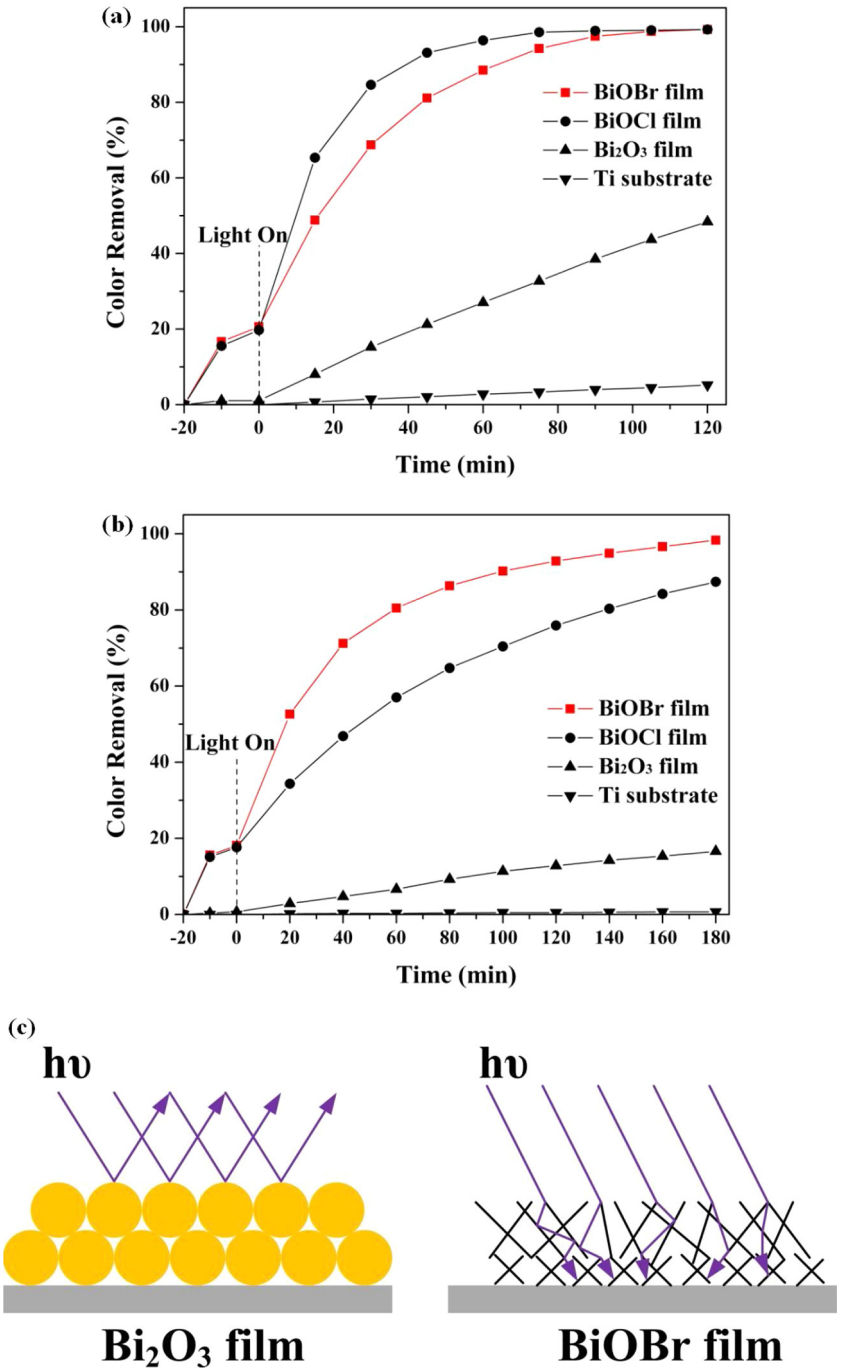

Fig. 5. The color removal of 50 mL 5 mg L^{-1} RhB using BiOBr film, BiOCl film and Bi_2O_3 film under (a) UV light and (b) visible light. (c) Schematic diagram of light reflection on the surface of Bi_2O_3 film and BiOBr film (rotating speed 60 rpm).

3.2. Optical absorption property of BiOBr film

The optical absorption properties of the semiconductor materials play a significant role in PC activity. The UV–vis diffuse reflectance spectra (DRS) of BiOBr film that prepared is shown in Fig. 4. The UV–vis DRS of BiOCl film is also presented for comparison. BiOBr film exhibited stronger absorption in the visible light region, and BiOCl film showed stronger UV light absorption. The onset of BiOBr was determined at 400 nm and the absorption edge occurred at about 450 nm. However, the absorption edge of BiOCl was found to be less than 370 nm. Because both the BiOBr and BiOCl are indirect transition semiconductors, the magnitude of band gap of BiOBr and BiOCl were estimated form a curve of $(\alpha h\upsilon)^{1/2}$ *vs.* photo energy ($h\upsilon$) with the help of Tauc relation. As shown the inset of Fig. 4, the band gap energy of BiOBr film was 2.5 eV, while the band gap of BiOCl film was 3.2 eV, which were both narrower than the theoretical values (2.7 eV for BiOBr and 3.4 eV for BiOCl). It is well known that the structure, morphology and the size of the semiconductor have an important influence on its optical properties [37]. The BiOCl film can only be excited by UV light due to its wide band gap energy, while the BiOBr film is suitable for visible light excitation due to its proper band gap energy. However, the narrower band gap energy of BiOBr indicates that the oxidation ability is becoming poorer than BiOCl.

3.3. PC activity of BiOBr on RhB removal

The PC activity of as-prepared BiOBr film was investigated by PC degradation of 50 mL 5 mg L^{-1} Rhodamine B (RhB) solution under UV and visible light, respectively, and the results are shown in Fig. 5. The Bi_2O_3 film and BiOCl film were also used to evaluate the PC performance of BiOBr film. The XRD and surface morphologies of these two films are shown in Fig. S1 and Fig. S2. As shown in Fig. 5, less than 5% RhB could be removed by photodegradation no matter under UV or visible light irradiation when Ti substrate was used without any photocatalyst immobilized.

The prepared Bi_2O_3 film is also an efficient photocatalyst that can be excited by part of visible light and the band gap energy (2.7 eV, Fig. S4) was even wider than that of BiOBr (2.5 eV), indicating stronger PC activity than that of BiOBr film. However, the RhB removal efficiency obtained by BiOBr film was much better than that obtained by Bi_2O_3, no matter under UV or visible light. This great improvement on RhB removal may mainly cause by the hierarchical structure of BiOBr film: (a) the hierarchical structure provides a larger surface area than Bi_2O_3 film which is built with solid nanospheres; (b) the hierarchical structure is benefit for RhB adsorption. About 20% RhB could adsorb on the surface of BiOBr film and no adsorption was observed on the surface of Bi_2O_3 film after 20 min adsorption; (c) the hierarchical structure can effectively capture more light [38,39]. This light harvesting property of BiOBr film can hardly be confirmed by direct data. Li et al. have synthesized similar hierarchical structured TiO_2 tubes and they have compared its PC activity with that of mechanically crushed sample [39]. Because the two samples had the same crystalline structure and the similar surface area, the dramatic activity enhancement mainly caused by the multiple reflections of incident light in this unique hierarchical structure. As shown in Fig. 5(c), when light irradiated, much of the light would reflect on the surface of Bi_2O_3 film and be wasted. However, for BiOBr film, much of the reflection light would be captured by the hierarchical structure. Furthermore, the inner layer of BiOBr film was more intensive than the outer layer, this double hierarchical structure may be more benefit for light capture.

Because both the BiOBr and BiOCl films own the hierarchical structure and exhibits similar RhB adsorption capacity, the comparison of BiOBr film and BiOCl film is more meaningful. As shown in Fig. 5(a), when UV light irradiated, the RhB removal efficiency obtained by BiOCl film was better than that obtained by BiOBr film. 83% color removal could be obtained by BiOCl film after 30 min UV irradiation, while about 70% RhB could be removed for BiOBr film. Because the band gap energy of BiOCl (3.2 eV) is wider than that of BiOBr (2.5 eV), the oxidation activity of BiOCl film is certainly stronger than that of BiOBr film. When visible light irradiated, as shown in Fig. 5(b), it was just the opposite that the RhB removal efficiency obtained by BiOBr film was much better than that obtained by BiOCl film. After 60 min irradiation, more than 80% RhB could be removed for BiOBr film, while less than 55% RhB was removed for BiOCl film. BiOCl can not be excited by visible light due to its wide band gap energy and RhB could only be removed through photosensitization process. This photosensitization degradation would also take place on the surface of BiOBr film due to its strong RhB adsorption capacity. However, because the band gap energy of BiOBr is suitable for visible light excitation, part of visible light could be utilized to excite BiOBr to direct oxidize RhB, which resulted in better RhB removal under visible light.

3.4. Stability of BiOBr film on RhB removal

The stability of obtained BiOBr film is an important factor that should be considered in real industrial application. As shown in Fig. 6, five runs of PC processes were repeated on one BiOBr film to treat 50 mL 5 mg L^{-1} RhB solution under 120 min UV light irradiation and 180 min visible light irradiation, respectively. The similar RhB removal efficiency obtained during each process demonstrates good stability and reliability of the BiOBr film.

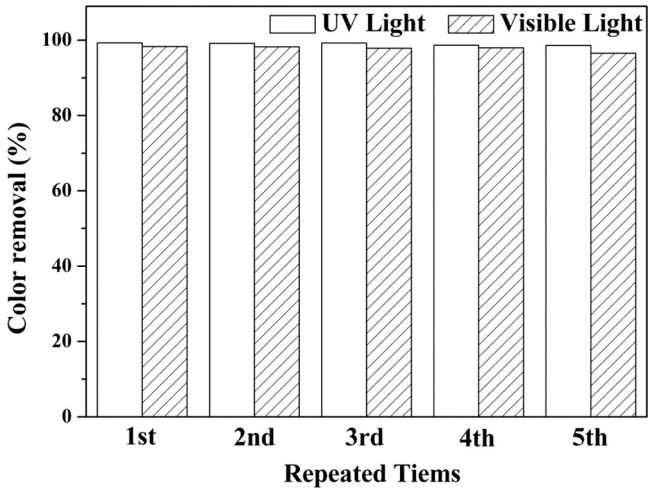

Fig. 6. Repeated removal of 50 mL 5 mg L^{-1} RhB solution with BiOBr film under 120 min UV light irradiation and 180 min visible light irradiation (rotating speed 60 rpm).

3.5. PC mechanisms of BiOBr film on RhB removal

In order to make clear the PC mechanisms of BiOBr film on RhB removal under UV and visible light, the effects of •OH and O_2•$^-$ radicals trapping agents were studied. As shown in Fig. 7(a), trapping •OH and O_2•$^-$ radicals with TBA and BQ both exhibited restraining effects on RhB color removal under UV light. This restraining effect was much stronger with the addition of TBA, indicating that •OH played a more important role in RhB color removal under UV light. BiOBr could be direct excited by UV light to generate electrons and holes. The photo generated holes could oxidize RhB directly or to oxidize H_2O to generate ·OH and further decompose RhB. The photo generated electrons were excited onto conduction band of BiOBr and reacted with O_2 to generate O_2•$^-$ to further oxidize RhB. However, compared with •OH (2.8 eV), the oxidation activity of O_2•$^-$ (1.7 eV) was much weaker.

When visible light irradiated, as shown in Fig. 7(b), it was just the opposite that O_2•$^-$ was the main active specie for RhB color removal. It was observed that the RhB degradation was also suppressed after trapping •OH under visible light, which was different from BiOCl film that RhB remained unchanged after the addition of TBA to trap •OH [18], suggesting that there was •OH generated on BiOBr film surface under visible light. Different from BiOCl, BiOBr could be excited by part of visible light to generate electrons and holes due to its narrower band gap energy (2.5 eV). In this case, •OH would be generated through decomposition of H_2O by photo generated holes. Besides this, similar with BiOCl, the RhB adsorption capacity was strong on the surface of BiOBr and RhB photosensitization degradation might also take place. In that case, RhB adsorbed on the surface of BiOBr film was excited by visible light and the excited electrons would inject into the conduction band of BiOBr and further react with O_2 to generate O_2•$^-$.

The effective electron injection and the subsequent formation of O_2•$^-$ require the good energy matching and enough redox potential of the conduction band of semiconductor [40]. For n-type semiconductor, the conduction band potential is very close to the flat-band potential (V_{fb}) and we have calculated the V_{fb} of BiOBr and BiOCl films through the Mott–Schottky plots. As shown in Fig. 7(c), both the BiOBr and BiOCl films belonged to n-type semiconductor [41].

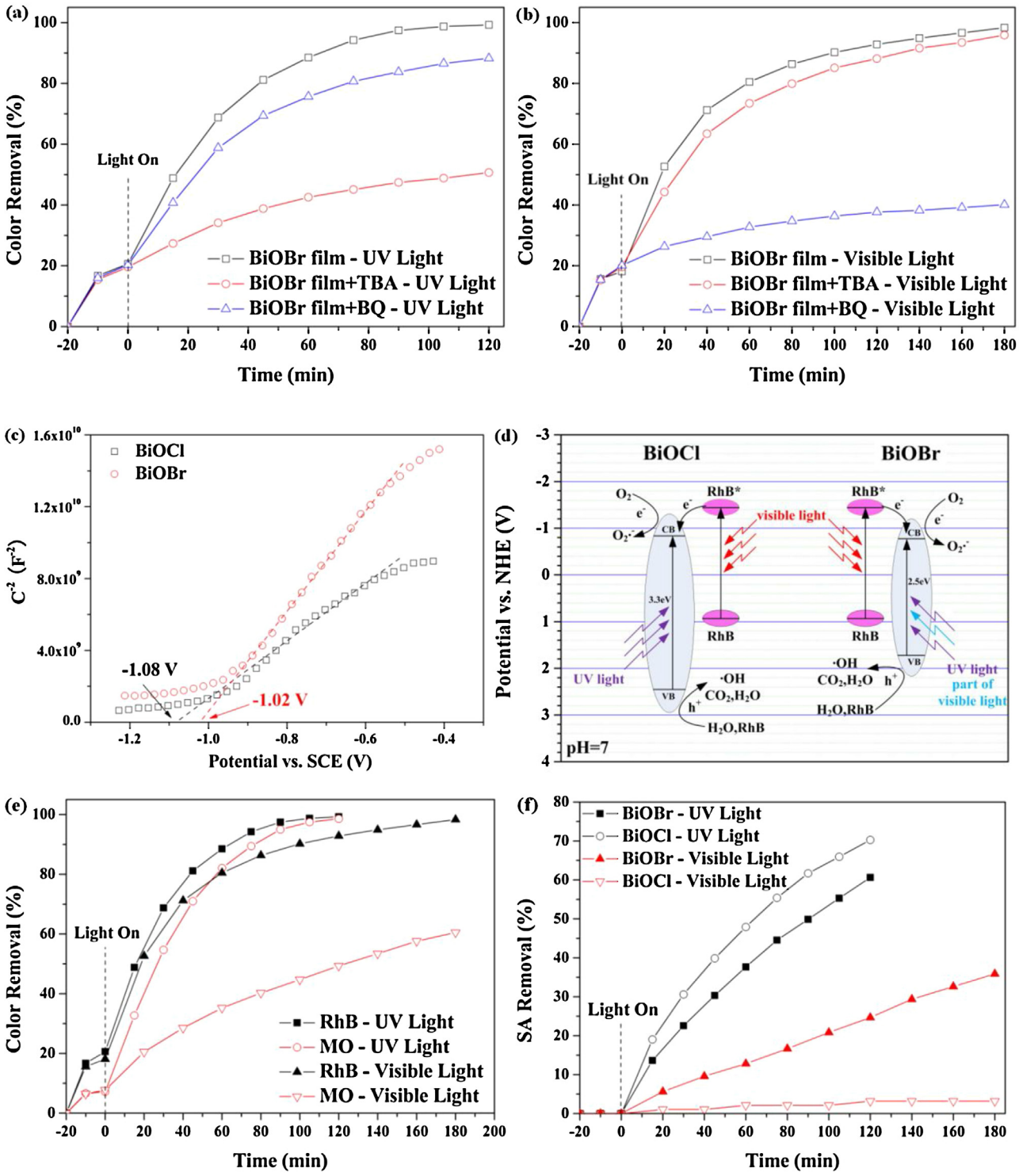

Fig. 7. Trapping experiments of active species during (a) UV and (b) visible light PC processes (TBA, •OH trapping agent; BQ, O_2•$^-$ trapping agent). (c) Mott–Schottky plots for BiOBr film and BiOBr film. (d) Photocatalytic mechanism schemes of BiOBr film and BiOCl film on RhB removal. (e) Comparison of PC degradation of 50 mL 5 mg L^{-1} RhB and MO under UV and visible light irradiation. (f) PC degradation of 50 mL 5 mg L^{-1} SA with BiOBr film and BiOCl film under UV and visible light irradiation. (Rotating speed 60 rpm).

The V_{fb} of BiOBr and BiOCl films were determined to be −1.02 V and −1.08 V *vs.* saturated calomel electrode (SCE), which were −0.78 V and −0.84 V *vs.* normal hydrogen electrode (NHE) at pH 7. Based on the band gap energy (2.5 eV for BiOBr and 3.2 eV for BiOCl), the valence band potential of BiOBr and BiOCl films were calculated to be 1.72 V and 2.36 V, respectively. The values of valence band edges suggested that the oxidation activity of BiOCl film was stronger than that of BiOBr film. Furthermore, it has been reported that the redox potentials of RhB and excited RhB* are 0.95 V and −1.42 V *vs.* NHE [42]. As shown in Fig. 7(d), the energy level of the excited RhB* was located well above the conduction bands of both BiOBr and BiOCl films, providing a favorable driving force for electron injection. Meanwhile, because the conduction bands of BiOBr and BiOCl films were more negative than E(O_2/O_2•$^-$) (−0.05 V), the injected

electrons could easily react with O_2 to generate $O_2\bullet^-$. According to above analysis, the PC mechanism of BiOBr film on RhB removal was summarized in Fig. 7(d). Similar with BiOCl film, photosensitization also took place on BiOBr film surface under visible light and played an important role on RhB degradation. While, different from BiOCl film, besides UV light, part of visible light could also excite BiOBr film to generate electrons and holes and further generate $O_2\bullet^-$ and •OH to oxidize RhB. Because the PC activity of BiOBr film was weaker than that of BiOCl film, RhB removal efficiency was lower than that obtained by BiOCl film under UV light (Fig. 5(a)). However, besides the photosensitization degradation, RhB could also be removed by hole and •OH direct oxidation, resulting in better RhB removal efficiency for BiOBr film under visible light (Fig. 5(b)).

In order to further confirm that both the photosensitization and direct photocatalysis took place for BiOBr film on RhB removal under visible light, 50 mL 5 mg L^{-1} Methyl Orange (MO, an anionic dye) and 50 mL 5 mg L^{-1} colorless salicylic acid (SA) were used instead of RhB to be treated by BiOBr film under UV and visible light. As shown in Fig. 7(e), when UV light irradiated, the color removal efficiencies of RhB and MO were similar for BiOBr film and the kinetic rates were 0.040 and 0.036, respectively (Fig. S5). Because •OH generated from H_2O oxidation was the main active species, excellent color removal efficiencies were obtained for both RhB and MO under UV irradiation. Meanwhile, the rotating disk PC reactor could utilize incident light more effectively, which also improved the color removal efficiency under UV irradiation. However, when visible light irradiated, the color removal efficiency of RhB was much better than that of MO and the kinetic rate was 3 times larger (Fig. S5). It is well known that dye adsorption is the prerequisite for photosensitization [43–45]. As shown in Fig. 7(e), the adsorption capacity of MO on BiOBr film was only 5% after 20 min adsorption, which was much less than that of RhB (20%). The zeta potential of BiOBr film was measured to be −18.4 mV, indicating the surface of BiOBr film was negative charged. RhB is a kind of cationic dye and could be adsorbed on the surface of BiOBr film easily through electrostatic interaction (Fig. S6(a)). In contrast, MO is a kind of anionic dye and could not be largely adsorbed on BiOBr film surface (Fig. S6(b)). This result confirmed that large amount of RhB was removed by photosensitization under visible light on the surface of BiOBr film.

For BiOBr film direct visible light excitation, as shown in Fig. 7(f), about 60% and 70% SA could be removed in 120 min under UV irradiation for BiOBr and BiOCl films, respectively, while 35% SA could also be removed in 180 min under visible light irradiation for BiOBr film, but less than 5% SA was degraded when BiOCl film was used. SA is colorless and no adsorption was observed, photosensitization would not take place under visible light. The degradation mainly resulted from the direct excitation of BiOBr film by visible light.

3.6. Electricity generation in BiOBr/Ti–Pt rotating disk PFC

A Pt cathode was connected to the BiOBr/Ti photoanode to establish a BiOBr/Ti–Pt rotating disk PFC. The electrons could transfer to Pt cathode from the external circuit due to the potential difference between the BiOBr/Ti photoanode and Pt cathode and react with O_2 at cathode. In this process, electricity was generated with degradation of pollutants simultaneously. The current–voltage (*J–V*) plots and the current–power (*J–JV*) plots obtained with 50 mL 5 mg L^{-1} RhB as "fuel" under UV and visible light are shown in Fig. 8. The open-circuit voltage (V_{OC}), short-circuit current density (J_{SC}), maximum power density (P_{max}) and fill factor (ff) of the PFC are listed in Table 1. The ff is calculated using the following equation [46]:

$$\mathrm{ff} = \frac{P_{max}}{J_{SC}V_{OC}} \quad (3)$$

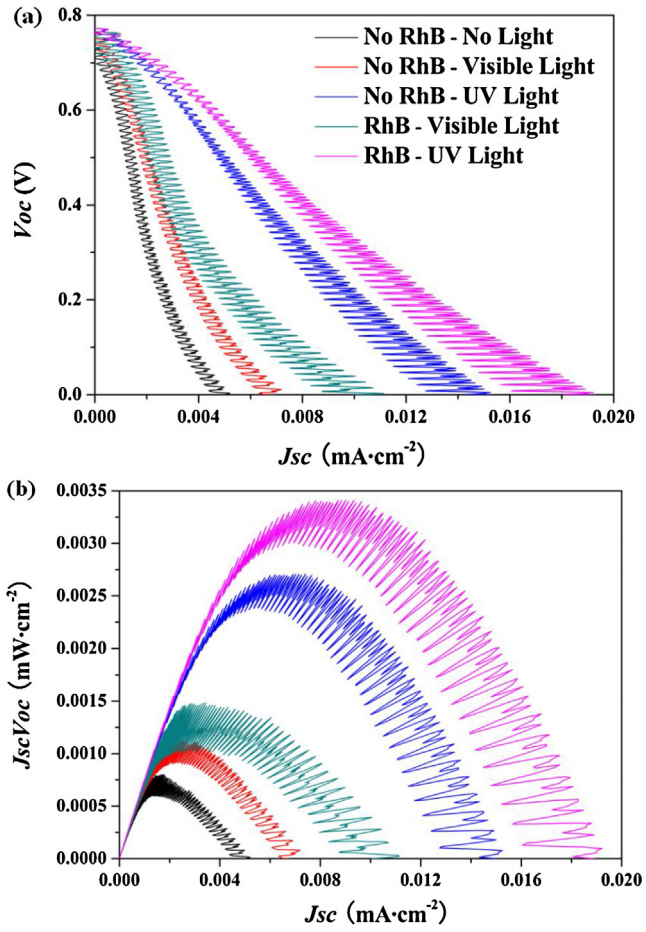

Fig. 8. (a) Current–voltage (*J–V*) plots and (b) current–power (*J–JV*) plots for BiOBr/Ti–Pt rotating disk PFC with 50 mL 5 mg L^{-1} RhB as "fuel" under UV and visible light irradiation (rotating speed 60 rpm, 0.05 mol L^{-1} NaBr as electrolyte).

The ff shows the deviation of the actual maximum power density produced by PFC from the value of $J_{SC}V_{OC}$, the product of the highest possible values of the current density and voltage. The performance of a PFC is directly related to its ff value, which should be optimized as high as possible [47].

When there was no light, the potential difference between BiOBr/Ti photoanode and Pt cathode was 0.72 V and the J_{SC} was 0.005 mA cm^{-2}. Because BiOBr film could be excited by both UV and visible light, the V_{OC} was enhanced to 0.77 V and 0.74 V under UV and visible light irradiation. Meanwhile, due to the transfer of photogeneration electrons, the J_{SC} was also improved to 0.015 and 0.006 mA cm^{-2},[2] respectively, in the absence of RhB. When RhB was added, because the V_{OC} is mainly generated from the chemical potential between the excited BiOBr photoanode and Pt cathode, no influence was observed on V_{OC}. However, more electrons would be generated and transfer to cathode due to the direct oxidation and the photosensitization of RhB on BiOBr/Ti photoanode, the J_{SC} was further improved to 0.019 mA cm^{-2} under UV light and 0.010 mA cm^{-2} under visible light. The current–time plots (Fig. 9(a)) showed that the total current generated was stable and gradually decreased with treatment time, which resulted from the consumption of RhB, or the "fuel". Besides the electricity generation, as shown in Fig. 9(b), RhB removal efficiency was also enhanced with the connection of Pt cathode both under UV and visible light. The photogenerated electrons and holes would easily separate and the recombination was restricted efficiently due to the potential difference generated between BiOBr/Ti

Table 1
Current–voltage (*J*–*V*) characteristics of the BiOBr/Ti–Pt rotating disk PFC with different fuels (rotating speed 60 rpm, 0.05 mol L^{-1} NaBr as electrolyte).

Fuel	V_{OC} (V)	J_{SC} (mA cm^{-2})	P_{max} (mW cm^{-2})	Ff
No fuel (UV)	0.77	0.015	0.0026	0.23
5 mg L^{-1} RhB (UV)	0.77	0.019	0.0033	0.23
0.005 mg L^{-1} Glucose (UV)	0.78	0.024	0.0043	0.23
0.05% Ethanol (UV)	0.78	0.025	0.0046	0.24
0.05% Acetic acid (UV)	0.78	0.028	0.0053	0.24
No fuel (vis)	0.74	0.006	0.0010	0.23
5 mg L^{-1} RhB (vis)	0.74	0.010	0.0014	0.19
0.005 mg L^{-1} Glucose (vis)	0.75	0.007	0.0021	0.40
0.05% Ethanol (vis)	0.75	0.007	0.0023	0.44
0.05% Acetic acid (vis)	0.75	0.009	0.0030	0.44

photoanode and Pt cathode, resulting in the enhancement of RhB removal efficiency.

Compare the ff values, we have found that the ff obtained under visible light (0.19) was lower than that obtained under UV light (0.23). It has been reported that the resistance and current leakage in PFC will greatly influence the electricity generation efficiency and ff value [48,49]. When UV light irradiated, the photogenerated electrons transferred to Ti substrate directly from the conduction band of BiOBr and further to Pt cathode from external circuit to generate electricity. However, when visible light irradiated, besides direct visible light excitation, large amount of electrons were generated by RhB photosensitization, these electrons had to inject to the conduction band of BiOBr first and then transfer to Ti substrate and further to Pt cathode from the external circuit to generate electricity. Because BiOBr was a semiconductor, more resistance would be generated during this process. Furthermore, due to the existence of resistance, electrons would accumulate at the interface between the adsorbed RhB and BiOBr, which might react with O_2 directly to generate $O_2\bullet^-$ and cause current leakage. The resistance and current leakage generated under visible light irradiation might decrease the ff value and turn the *J*–*V* plot to a concave shape [50].

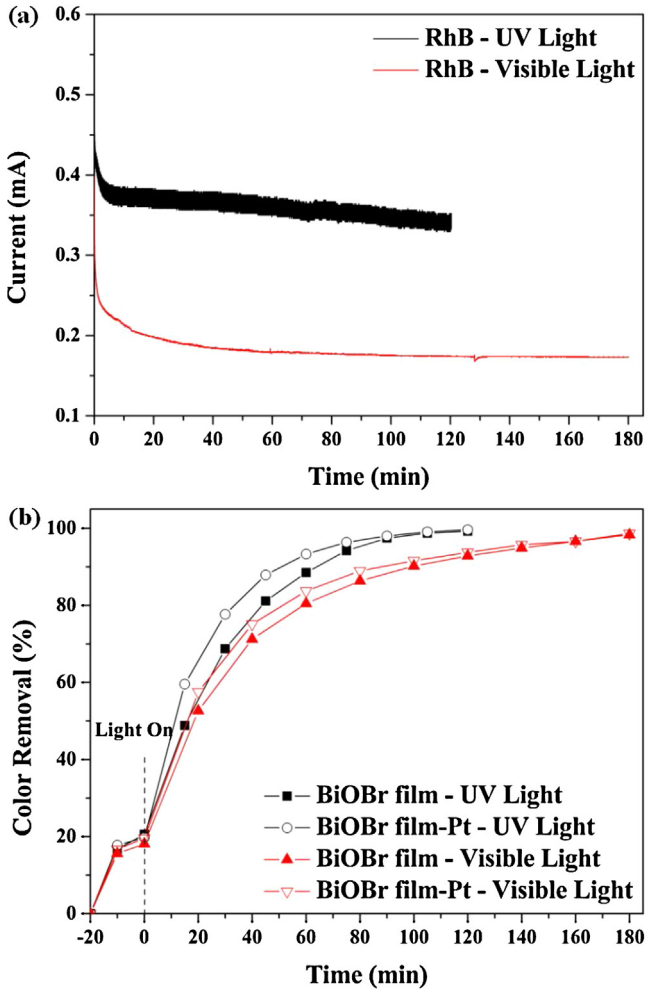

Fig. 9. (a) Current–time plots of BiOBr/Ti–Pt rotating disk PFC with 50 mL 5 mg L^{-1} RhB as "fuel" under UV and visible light irradiation. (b) The color removal of 50 mL 5 mg L^{-1} RhB with and without connection of Pt cathode in BiOBr/Ti–Pt rotating disk PFC (rotating speed 60 rpm, 0.05 mol L^{-1} NaBr as electrolyte).

Other easily oxidized organic compounds including glucose, ethanol and acetic acid with high concentrations were also employed by us to evaluate the electricity generation properties in BiOBr/Ti–Pt rotating disk PFC. As shown in Table 1 and Fig. S7, the V_{OC} was slightly enhanced to 0.78 and 0.75 V under UV and visible light irradiation. Because the oxidation of glucose, ethanol and acetic acid is more easily than RhB and the concentration of these compounds were much higher, the J_{SC} generated under UV light was greatly improved from 0.019 mA cm^{-2} to 0.024, 0.025 and 0.028 mA cm^{-2}. When visible light irradiated, because photosensitization did not take place for these compounds, the J_{SC} was lower than that obtained by RhB as "fuel". However, when these compounds were used as "fuels", the resistance and the current leakage were lower under visible light irradiation in comparison with RhB and the ff was enhanced from 0.19 to more than 0.40.

4. Conclusion

A double hierarchical structured BiOBr film was prepared on a Ti substrate and was equipped on a rotating disk PC reactor to evaluate its PC activity. The prepared BiOBr film exhibited much better PC activity on RhB removal than Bi_2O_3 film under UV and visible light. The double hierarchical structure could not only enhance the surface area, but also exhibited strong RhB adsorption capacity and high light utilization efficiency due to multiple reflections of incident light. Compared with BiOCl film with similar hierarchical structure, the RhB removal efficiency was little bit lower under UV light because the oxidation activity of BiOBr (2.5 eV) was weaker than that of BiOCl (3.2 eV). However, much better RhB removal efficiency was obtained for BiOBr film under visible light irradiation. Besides RhB photosensitiazation degradation, the narrower band gap energy of BiOBr (2.5 eV) made it can be directly excited by part of visible light to generate ·OH. A Pt cathode was further connected to BiOBr/Ti photoanode to establish a BiOBr/Ti–Pt rotating disk photoelectrochemical cell to generate electricity with degradation of pollutants simultaneously. 0.77 and 0.74 V open-circuit voltage, 0.019 and 0.010 mA cm^{-2} short-circuit current density could be obtained under UV and visible light with 50 mL 5 mg L^{-1} RhB as "fuel", respectively. Because the recombination of electrons and holes could be restricted due to the effective

transfer of photogenerated electrons to Pt cathode through external circuit, the photocatalytic activity was also improved both under UV and visible light. The total current generated was stable but gradually decreased with treatment time due to the consumption of "fuel".

Acknowledgements

Financial support from the National Natural Science Foundation of China (Project No. 21477076 and 20937003), China Postdoctoral Science Foundation (No. 2013M540370) and Shanghai Tongji Gao Tingyao Environmental Science & Technology Development Foundation are gratefully acknowledged.

Appendix A. Supplementary data

Supplementary data associated with this article can be found, in the online version, at http://dx.doi.org/10.1016/j.apcatb.2014.09.017.

References

[1] J. Mo, Y. Zhang, Q. Xu, J.J. Lamson, R. Zhao, Atmos. Environ. 43 (2009) 2229–2246.
[2] J. Chen, C. Poon, Build. Environ. 44 (2009) 1899–1906.
[3] N. Keller, M.-N. Ducamp, D. Robert, V. Keller, Chem. Rev. 113 (2013) 5029–5070.
[4] Y. Lai, Y. Tang, J. Gong, D. Gong, L. Chi, C. Lin, Z. Chen, J. Mater. Chem. 22 (2012) 7420–7426.
[5] Y. Paz, Appl. Catal., B—Environ. 99 (2010) 448–460.
[6] D.D. Dionysiou, G. Balasubramanian, M.T. Suidan, A.P. Khodadoust, I. Baudin, J.-M. Laîné, Water Res. 34 (2000) 2927–2940.
[7] Y. Yao, K. Li, S. Chen, J. Jia, Y. Wang, H. Wang, Chem. Eng. J. 187 (2012) 29–35.
[8] K. Li, Y. He, Y. Xu, Y. Wang, J. Jia, Environ. Sci. Technol. 45 (2011) 7401–7407.
[9] K. Li, C. Yang, Y. Wang, J. Jia, Y. Xu, Y. He, AIChE J. 58 (2012) 2448–2455.
[10] D. Zhang, M. Wen, S. Zhang, P. Liu, W. Zhu, G. Li, H. Li, Appl. Catal., B—Environ. 147 (2014) 610–616.
[11] J.B. Joo, M. Dahl, N. Li, F. Zaera, Y. Yin, Energy Environ. Sci. 6 (2013) 2082–2092.
[12] H. Guo, W. Wang, L. Liu, Y. He, C. Li, Y. Wang, Green Chem. 15 (2013) 2810–2816.
[13] M. Guan, C. Xiao, J. Zhang, S. Fan, R. An, Q. Cheng, J. Xie, M. Zhou, B. Ye, Y. Xie, J. Am. Chem. Soc. 135 (2013) 10411–10417.
[14] Q.-C. Liu, D.-K. Ma, Y.-Y. Hu, Y.-W. Zeng, S.-M. Huang, ACS Appl. Mater. Inter. 5 (2013) 11927–11934.
[15] W. Zhang, Q. Zhang, F. Dong, Ind. Eng. Chem. Res. 52 (2013) 6740–6746.
[16] K. Zhang, J. Liang, S. Wang, J. Liu, K. Ren, X. Zheng, H. Luo, Y. Peng, X. Zou, X. Bo, J. Li, X. Yu, Cryst. Growth Des. 12 (2012) 793–803.
[17] Y. Huo, J. Zhang, M. Miao, Y. Jin, Appl. Catal., B—Environ. 111–112 (2012) 334–341.
[18] K. Li, Y. Tang, Y. Xu, Y. Wang, Y. Huo, H. Li, J. Jia, Appl. Catal. B—Environ. 140–141 (2013) 179–188.
[19] Y. Fang, Y. Huang, J. Yang, P. Wang, G. Cheng, Environ. Sci. Technol. 45 (2011) 1593–1600.
[20] H. Tian, J. Li, M. Ge, Y. Zhao, L. Liu, Catal. Sci. Technol. 2 (2012) 2351–2355.
[21] Y. Chen, M. Wen, Q. Wu, CrystEngComm 13 (2011) 3035–3039.
[22] L. Li, L. Ai, C. Zhang, J. Jiang, Nanoscale 6 (2014) 4627–4634.
[23] Z. Xu, L. Han, B. Lou, X. Zhang, S. Dong, Nanoscale 6 (2014) 145–150.
[24] Y. Xu, Y. He, X. Cao, D. Zhong, J. Jia, Environ. Sci. Technol. 42 (2008) 2612–2617.
[25] M. Kaneko, J. Nemoto, H. Ueno, N. Gokan, K. Ohnuki, M. Horikawa, R. Saito, T. Shibata, Electrochem. Commun. 8 (2006) 336–340.
[26] P. Lianos, J. Hazard. Mater. 185 (2011) 575–590.
[27] M. Antoniadou, S. Sfaelou, P. Lianos, Chem. Eng. J. 254 (2014) 245–251.
[28] B. Seger, G.Q. Lu, L. Wang, J. Mater. Chem. 22 (2012) 10709–10715.
[29] D. Shu, J. Wu, Y. Gong, S. Li, L. Hu, Y. Yang, C. He, Catal. Today 224 (2014) 13–20.
[30] K. Li, Y. Xu, Y. He, C. Yang, Y. Wang, J. Jia, Environ. Sci. Technol. 47 (2013) 3490–3497.
[31] K. Li, H. Zhang, T. Tang, Y. Xu, D. Ying, Y. Wang, J. Jia, Water Res. 62 (2014) 1–10.
[32] Y. Du, Y. Feng, Y. Qu, J. Liu, N. Ren, H. Liu, Environ. Sci. Technol. 48 (2014) 7634–7641.
[33] C. Pan, Y. Zhu, Environ. Sci. Technol. 44 (2010) 5570–5574.
[34] L. Ye, J. Liu, C. Gong, L. Tian, T. Peng, L. Zan, ACS Catal. 2 (2012) 1677–1683.
[35] D. Zhang, J. Li, Q. Wang, Q. Wu, J. Mater. Chem., A 1 (2013) 8622–8629.
[36] S. Cao, C. Guo, Y. Lv, Y. Guo, Q. Liu, Nanotechnology 20 (2009) 275702.
[37] G. Dukovic, F. Wang, D. Song, M.Y. Sfeir, T.F. Heinz, L.E. Brus, Nano Lett. 5 (2005) 2314–2318.
[38] Y. Huo, X. Chen, J. Zhang, G. Pan, J. Jia, H. Li, Appl. Catal., B—Environ. 148–149 (2014) 550–556.
[39] G. Li, J. Liu, G. Jiang, Chem. Commun. 47 (2011) 7443–7445.
[40] J. Hu, W. Fan, W. Ye, C. Huang, X. Qiu, Appl. Catal., B—Environ. 158–159 (2014) 182–189.
[41] S. Weng, B. Chen, L. Xie, Z. Zheng, P. Liu, J. Mater. Chem., A 1 (2013) 3068–3075.
[42] Z. Xiong, L.L. Zhang, J. Ma, X.S. Zhao, Chem. Commun. 46 (2010) 6099–6101.
[43] X. Qian, K. Fuku, Y. Kuwahara, T. Kamegawa, K. Mori, H. Yamashita, ChemSusChem 7 (2014) 1528–1536.
[44] X.F. Qian, T. Kamegawa, K. Mori, H.X. Li, H. Yamashita, J. Phys. Chem. C 117 (2013) 19544–19551.
[45] Y. Kuwahara, H. Yamashita, J. Mater. Chem. 21 (2011) 2407–2416.
[46] B. O'Regan, M. Grätzel, Nature 353 (1991) 737–740.
[47] D. Gupta, S. Mukhopadhyay, K.S. Narayan, Sol. Energy Mat. Sol., C 94 (2010) 1309–1313.
[48] B.D. Yuhas, P. Yang, J. Am. Chem. Soc. 131 (2009) 3756–3761.
[49] L. Yang, T. Zhang, H. Zhou, S.C. Price, B.J. Wiley, W. You, ACS Appl. Mater. Int. 3 (2011) 4075–4084.
[50] D. Gupta, M. Bag, K.S. Narayan, Appl. Phys. Lett. 92 (2008) 093301.